

Article

A Mathematical Model of Spontaneous Action Potential Based on Stochastic Synaptic Noise Dynamics in Non-Neural Cells

Chitaranjan Mahapatra ^{1,2,*}  and Inna Samuilik ³ ¹ Cardiovascular Research Institute, University of California San Francisco, San Francisco, CA 94115, USA² Biomedical Engineering, Indian Institute of Technology Bombay, Mumbai 400076, India³ Institute of Applied Mathematics, Riga Technical University, LV-1048 Riga, Latvia; inna.samuilika@rtu.lv

* Correspondence: cmahapatra97@gmail.com or chitaranjan@iitb.ac.in

Abstract: We developed a mathematical model to simulate the dynamics of background synaptic noise in non-neuronal cells. By employing the stochastic Ornstein–Uhlenbeck process, we represented excitatory synaptic conductance and integrated it into a whole-cell model to generate spontaneous and evoke cellular electrical activities. This single-cell model encompasses numerous biophysically detailed ion channels, depicted by a set of ordinary differential equations in Hodgkin–Huxley and Markov formalisms. Consequently, this approach effectively induced irregular spontaneous depolarizations (SDs) and spontaneous action potentials (sAPs), resembling electrical activity observed in vitro. The input resistance decreased significantly, while the firing rate of spontaneous action potentials increased. Moreover, alterations in the ability to reach the action potential threshold were observed. Background synaptic activity can modify the input/output characteristics of non-neuronal excitatory cells. Hence, suppressing these baseline activities could aid in identifying new pharmaceutical targets for various clinical diseases.

Keywords: excitable cells; synaptic conductance; stochastic synaptic noise; noise dynamics; action potential; mathematical modeling

MSC: 37M05

**Citation:** Mahapatra, C.; Samuilik, I.

A Mathematical Model of Spontaneous Action Potential Based on Stochastic Synaptic Noise Dynamics in Non-Neural Cells.

Mathematics **2024**, *12*, 1149. <https://doi.org/10.3390/math12081149>

Received: 3 March 2024

Revised: 7 April 2024

Accepted: 10 April 2024

Published: 11 April 2024



Copyright: © 2024 by the authors. Licensee MDPI, Basel, Switzerland. This article is an open access article distributed under the terms and conditions of the Creative Commons Attribution (CC BY) license (<https://creativecommons.org/licenses/by/4.0/>).

1. Introduction

Electrically excitable cells such as neurons, cardiac cells, skeletal muscle cells, and smooth muscle cells generate membrane depolarization and action potential (AP) to initiate various physiological functions and information exchange between cells [1]. Action potential or spike initiation in excitable cells adheres to the all-or-none principle, which states that characteristic action potential is generated and sent when the cell is adequately stimulated, and no spike is triggered if the potential is below the threshold [2]. Specific ion channels are activated at a particular threshold potential, which is the crucial factor responsible for generating spikes [3]. The membrane is depolarized till the threshold potential is reached by several mechanisms, which are illustrated in Figure 1. The elevation of transient membrane depolarization is denoted by ΔV .

The membrane can depolarize when positive ions accumulate in the intracellular space as a result of the opening of particular ion channels: nonspecific cation channels (NSCCs), voltage-dependent calcium channels (VDCCs), and voltage-gated sodium channels (Navs) [4]. The voltage-gated potassium channel (Kv) repolarizes the membrane potential by moving positive ions out of the cell [5–7]. Additionally, the transmission of the electrical potential from one cell to another (from cell 2 to cell 1) through a gap junction can cause membrane depolarization [8]. Furthermore, certain cells are myogenic, meaning that they contain interstitial cells of Cajal (ICC) which are pace-making cells that can depolarize the membrane through self-activation [9]. In another neurogenic process mechanism, the release of various neurotransmitters with excitatory or inhibitory synaptic conductance

can either depolarize or hyperpolarize the membrane potential, either through triggered or spontaneous events [10]. The nervous system innervates most excitable cells, making this process crucial in various pathophysiological conditions. Neurotransmitter release from the synapse is orchestrated by the nervous system. Electrical activities involving stochastic neurotransmitter release occur as background events in the intracellular recordings of excitable cells [11]. The primary contributors to the inherent variability observed in excitable cells within microcircuits and networks stem from the probabilistic nature of ion channel gating and the initiation of synaptic conductances [12–15]. Research investigations have utilized diverse approaches, including *in vivo*, *in vitro*, and computational modeling techniques, to analyze the impact of synaptic background activity on neuronal cells. Nevertheless, this research was not adequately explored in non-neuronal excitatory cells, such as cardiac and smooth muscle cells, where neurotransmitter-based innervation also occurs. The primary physiological function of the urinary bladder, a component of the urinary system, is to facilitate the process of micturition, which involves storing and releasing urine. The parasympathetic nervous system being activated by signals from the brain and spinal cord triggers the contraction of detrusor smooth muscle (DSM) cells, thereby facilitating the micturition process. The DSM is highly innervated, linking around 16,000 afferent and efferent axons from ganglion neurons across different species [16–18]. Research conducted over the past 50 years has established that DSM cells exhibit spontaneous phasic contraction activities through spontaneously evoked depolarizations (SDs) and action potentials (sAPs) [18–20]. Intracellular recordings from mouse DSM cells also show characteristics of SDs and sAPs [18,21–23]. The neurogenic hypothesis proposes that the elevation of the resting membrane potential (RMP) due to spontaneous neurotransmitter release and the interplay of inherent ion channels within the DSM cell membrane play significant roles in initiating sAPs and SDs [18,24–27]. According to Young et al. (2008) [18], ATP, acting as a purinergic neurotransmitter, is released sporadically into the DSM cells from parasympathetic nerve terminals. Varicosities located at these terminals generate ATP, which subsequently triggers P2X receptors on the DSM cell membrane. This activation facilitates the influx of cation X^+ through a metabotropic mechanism. At times, the increase in X^+ leads to enough membrane depolarization to trigger voltage-dependent calcium channels across the membrane. Therefore, an in-depth understanding of membrane biophysics, particularly the mechanism of neurotransmitter activation, might lead to new pharmacological innovations for pathological disorders such as overactive bladder and urinary incontinence. However, due to complexity, studies using *in vivo* and *in vitro* methods to investigate the precise impact of synaptic activity have not adequately addressed non-neuronal excitatory cells, especially in smooth muscles like those found in the DSM cells.

Mathematical modeling methods are essential for quantitatively studying complicated biological processes [28]. Modeling intracellular electrophysiological processes creates a virtual physiological system that can be used to study the impact of different pharmaceutical targets on excitable cells [29]. Many mathematical models have been used to study the cellular excitability qualities of neuronal cells influenced by synaptic background noise [30]. These models are restricted to non-neuronal cells such as heart cells and smooth muscle cells. The present computational study aims to enhance our understanding of the impact of synaptic background activities on DSM cell excitability. This is achieved by simulating the spontaneous intracellular electrical properties resulting from the addition of continuous fluctuating conductances at synapses. Excitable and densely innervated cells are recognized for potentially displaying substantial synaptic conductances due to neurotransmitter leakage [31]. DSM tissue also falls within this classification, as indicated by Gabella, G. in 1999 [19] and corroborated by the last paragraph. The Ornstein–Uhlenbeck process is a stochastic process widely utilized across diverse fields, including finance, physics, and biology. It also serves as a model where background activity imitates continuous synaptic conductance activities for modulating neuron firing rates and patterns [32–34]. We have refined these models, incorporating precise adjustments to simulate the modulatory impact

of stochastic excitatory synaptic conductance on spontaneous electrical activities within the previously published biophysically detailed DSM cell models [35–39].

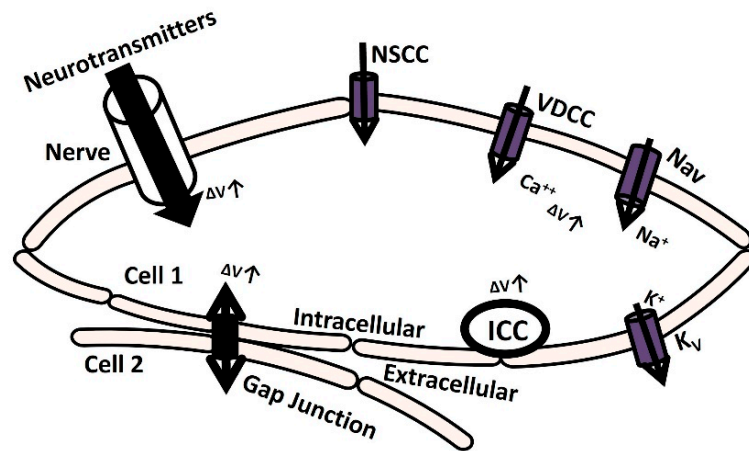


Figure 1. The schematic diagram illustrates cellular mechanisms for membrane depolarization. It delineates how membrane depolarization occurs through the release of neurotransmitters, the activation of ion channels, and the establishment of gap junction connections with adjacent cells. Further elucidation is provided in the subsequent paragraph.

2. Materials and Methods

A model utilizing point conductance was developed to mimic the background activity in DSM cells driven by neurotransmitters. In this model, Equation (1) treated the neurotransmitter current I_{nt} as an independent excitatory conductance:

$$I_{nt} = g_{ex}(V - E_{ex}) \tag{1}$$

where $g_{ex}(t)$ is the time-dependent excitatory conductance, V is the membrane potential, and E_{ex} is the excitatory neurotransmitter reversal potential.

Equation (2) characterizes the excitatory conductance $g_{ex}(t)$ as a single-variable stochastic process:

$$\frac{dg_{ex}(t)}{dt} = -\frac{1}{\tau_{ex}} [g_{ex}(t) - g_{ex0}] + \sqrt{D_{ex}} \lambda_1(t) \tag{2}$$

In the given context, g_{ex0} represents the mean conductance, τ_{ex} denotes the time constants, D_{ex} signifies the diffusion coefficients utilized for noise generation, and $\lambda_1(t)$ represents Gaussian white noise. The numerical integration technique employed for solving the differential equations is derived from [32–34].

The DSM cell model integrates the point conductance within a solitary cylindrical compartment [35,37]. Active ion channels are represented using the Hodgkin–Huxley formulation [40]. The DSM cell membrane is conceptualized as a model based on conductance, incorporating various ion channel conductances that can change over time, along with a membrane capacitance C_m . Figure 2 depicts the schematic overview of ion channel mechanisms in individual DSM cells (a) and illustrates a schematic overview of the parallel conductance model for the ionic current (b).

In the single DSM cell model (Figure 2a), $PMCA$, I_{CaT} , I_{CaL} , I_{KCa} , I_{Kv} , I_{Leak} , and I_h are known as the Ca^{2+} pump, T-type Ca^{2+} channel, L-type Ca^{2+} channel, Ca^{2+} -dependent K^+ channel, voltage-dependent K^+ channel, leakage channel, and hyperpolarization-activated cation current, respectively. The parallel conductance model (Figure 2b) illustrates the flow of ion ‘ X^+ ’ under the influence of an electrochemical driving force. The series connection of ion channel conductance g_{ion} and the ion channel’s Nernst potential E_{ion} are connected parallelly to the membrane capacitance C_m . The dimensions of the single cylindrical compartment are specified as 200 μm in length and 6 μm in diameter. To model the passive electrical properties, values for membrane capacitance (C_m), membrane resistance

(R_m), and axial resistance are utilized, set at $1 \mu\text{F}/\text{cm}^2$, $138 \text{M}\Omega\text{-cm}^2$, and $181 \Omega\text{-cm}$ [41], respectively.

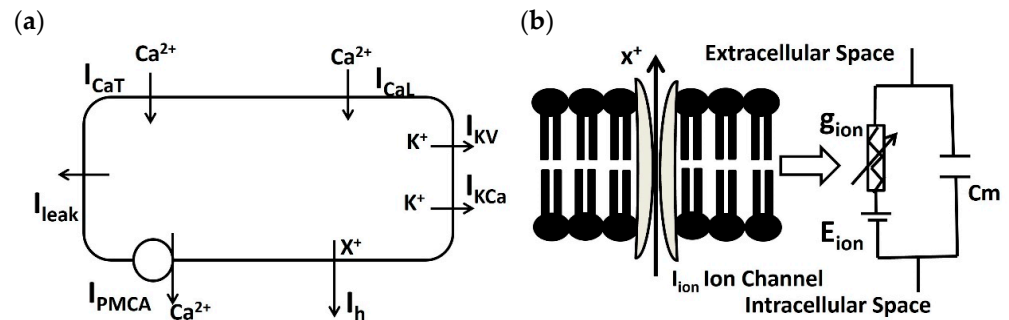


Figure 2. (a) Schematic overview of ion channel mechanisms (PMCA, I_{CaT} , I_{CaL} , I_{KCa} , I_{KV} , I_{Leak} , and I_h) in the isolated DSM model. (b) A diagram illustrating the parallel conductance model for the ionic current is presented schematically. It represents the flow of ion X using g_{ion} , C_m , and R_m . Further elucidation is provided in the subsequent paragraph.

The time dependence characteristics of the membrane potential (V_m) are represented in Equation (1).

$$\frac{dV_m(t)}{dt} = - \left[\frac{I_{ion}(t) + I_{stim}(t)}{C_m} \right] \quad (3)$$

where C_m is the membrane capacitance.

If we apply a stimulus current I_{stim} and Kirchhoff's current law, the differential equation in Equation (4) will be formed to describe the changes in transmembrane potential V_m :

$$\left(\frac{dV_m}{dt} \right) = - \left(\frac{1}{C_m} (I_{Ca} + I_K + I_h + I_{leak} + I_{stim}) \right) \quad (4)$$

Most of the ion channel currents are built according to the most conventional Hodgkin-Huxley (HH) formulation:

$$I = \bar{g} [m(V_m, t, [Ca^{2+}]_i)]^x h[(V_m, t, [Ca^{2+}]_i)]^y (V_m - E_{rev}) \quad (5)$$

where \bar{g} and E_{rev} are the maximum conductance and Nernst potential of the particular ion channel, respectively; E_{rev} is the ion's reversal potential; 'm' and 'h' are the dimensionless gating variables to denote the time/voltage/ Ca^{2+} -dependent activation and time/voltage/ Ca^{2+} -dependent inactivation of the channel conductance. The 'x' and 'y' values are power levels corresponding to the functions.

The change in each gating variable (m or h) can be described by a first-order differential equation, as indicated by Equations (6) and (7):

$$\frac{dm(V_m, t)}{dt} = \frac{m_\infty(V_m) - m(V_m, t)}{\tau_m} \quad (6)$$

$$\frac{dh(V_m, t)}{dt} = \frac{h_\infty(V_m) - h(V_m, t)}{\tau_h} \quad (7)$$

In this context, m_∞ and h_∞ represent the steady-state values, while τ_m , and τ_h denote the time constants, which vary depending on the voltage and/or intracellular Ca^{2+} ionic concentrations.

The relationship between the state parameters and the membrane potential (V_m) for ion channels is elucidated by the Boltzmann equation:

$$m_\infty(V_m, t) = \frac{1}{1 + \exp\left(\frac{V_m + V_{m\frac{1}{2}}}{S_m}\right)} \quad (8)$$

$$h_{\infty}(V_m, t) = \frac{1}{1 + \exp\left(\frac{V_m + V_{h\frac{1}{2}}}{S_h}\right)} \tag{9}$$

where $V_{1/2}$ represents the half-activation potential and S denotes the slope factor.

The kinetics of large conductance Ca^{2+} -activated K^+ (BK) channels are characterized by a detailed multiple-state Markov model (MM), enhancing precision in modeling the channel's Ca^{2+} dependency. Our single-cell model integrates a 10-state MM, as depicted in Figure 3, to accurately simulate the BK channel current. This model comprises five closed "horizontal" conformation states (C0–C4) and five open-oriented "horizontal" states (O0–O4), each corresponding to its respective closed state. Notably, the open-state O4 enables the passage of K^+ ions through BK channels due to the instantaneous electrochemical driving force (EDF).

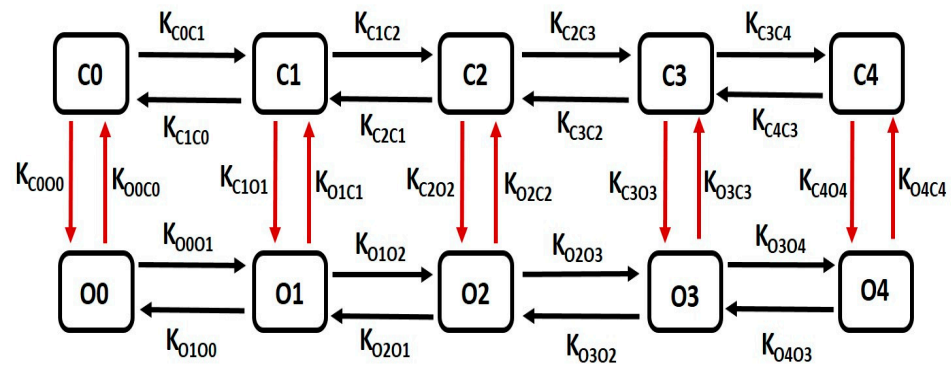


Figure 3. The schematic diagram illustrates a 10-state Markov model for the BK channel. It includes five closed "horizontal" conformation states labeled as C0, C1, C2, C3, and C4, and five open-oriented "horizontal" conformation states labeled as O0, O1, O2, O3, and O4, with each corresponding to the respective closed state. Further details on this model are elaborated in the following paragraph.

Equation (10) is utilized to compute the BK current (I_{BK}):

$$I_{BK} = \overline{g_{BK}} * O * (V - E_K) \tag{10}$$

where $\overline{g_{BK}}$ is referred to as the maximal conductance, and 'O' represents the sum of 'O1', 'O2', 'O3', and 'O4'

The common rate equations are as follows:

$$K_{on} = 345, K_{coff} = 25, K_{off} = 25, O = O1 + O2 + O3 + O4 \tag{11}$$

The rate equations for voltage-dependent transitions are as follows:

$$K_{C0O0} = 0.02162 * a, K_{C1O1} = 0.000869 * a, K_{C2O2} = 0.0000281 * a, K_{C3O3} = 0.000781 * a, K_{C4O4} = 0.044324 * a, K_{O0C0} = 318.1084 * b, K_{O1C1} = 144.1736 * b, K_{O2C2} = 32.6594 * b, K_{O3C3} = 0.095312 * b, K_{O4C4} = 0.000106 * b * cai \tag{12}$$

The state equations for calcium-dependent transitions are as follows:

$$K_{C0C1} = 4 * K_{on} * cai, K_{C1C2} = 3 * K_{on} * cai, K_{C2C3} = 2 * K_{on} * cai, K_{C3C4} = K_{on} * cai, K_{C4C3} = 4 * K_{coff} * cai, K_{C3C2} = 3 * K_{coff} * cai, K_{C2C1} = 2 * K_{coff} * cai, K_{C1C0} = K_{coff} * cai, K_{O0O1} = 4 * K_{on} * cai, K_{O1O2} = 3 * K_{on} * cai, K_{O2O3} = 2 * K_{on} * cai, K_{O3O4} = K_{on} * cai, K_{O4O3} = 4 * K_{off} * cai, K_{O3O2} = 3 * K_{off} * cai, K_{O2O1} = 2 * K_{off} * cai, K_{O1O0} = K_{off} * cai \tag{13}$$

The numbers associated with the state equations are selected to achieve precise BK current measurements during voltage-clamp protocols.

The calcium-dependent intermediate potassium current in (I_{IK}) in [35] is modified with the following equations.

$$I_{IK} = \overline{g_{IK}} * l^2 * k * (V - E_K) \quad (14)$$

$$l_{\infty} = \frac{0.37}{1 + \exp\left(\frac{(li-v)}{16}\right)} \quad (15)$$

$$li = -180 + (38 * \exp^{(ci*60)}) + (86 * \exp^{(-27*ci)}) \quad (16)$$

$$\tau_l = 17 * \left(\frac{30}{1 + \exp\left(\frac{(V+20.52)}{36}\right)}\right) \quad (17)$$

$$k_{\infty} = \frac{0.36}{1 + \exp\left(\frac{(67+v)}{9}\right)} \quad (18)$$

$$\tau_k = 55 * \left(1 - \frac{1}{\left(1 + \exp\left(\frac{(v+13.9629)}{45.3782}\right)\right) * \left(1 + \exp\left(\frac{-(v+9.49866)}{3.3945}\right)\right)}\right) \quad (19)$$

In our DSM cell model, action potentials were initiated through the external stimulus current (I_{st}) or the synaptic input-derived current (I_{syn}). I_{st} was administered as a brief rectangular pulse for single action potentials or prolonged rectangular pulses for multiple action potentials. Simulations utilized a fixed time step of 0.04 ms via the Euler method on a PC with an Intel Core i7 CPU operating at 3.80 GHz with a dual-core processor. The model utilizes the NEURON [42] simulation environment, known for its widespread usage in the realistic modeling of excitable cells. The Euler method is a basic numerical approach used to solve ordinary differential equations (ODEs). NEURON software 8.2.3 version offers stability and flexibility in simulating neuron dynamics, and the Euler method is used for solving ODEs due to its simplicity and efficiency [42]. NEURON primarily employs implicit integration methods (such as backward Euler) and a Crank–Nicolson variants for stability purposes [42], but it also allows the use of Euler’s method when appropriate, especially for its low memory requirements and ease of implementation [42].

After developing the model, we assessed its stability and reproducibility to variations in intrinsic parameters. This involved systematically adjusting the maximum conductance (g_{max}) of each ionic conductance within a range of $\pm 30\%$ of its default value. Our findings revealed that the simulated APs remained stable amidst such changes. While the AP and depolarization characteristics responded predictably to alterations in conductance (e.g., increasing the g_{max} of inward current ion channels resulted in higher AP peak amplitudes), the AP maintained its integrity without experiencing any pathological deviations in amplitude or waveform parameters.

The model code will be available in GitHub and the repository (<https://modeldb.science/> (accessed on 1 April 2024)) for free code sharing.

3. Results

In the Results section of our simulation, we accurately reproduced all types of electrical activities in the DSM cell, both with and without noise conductance. Our investigation focused on the membrane excitability properties resulting from spontaneous purinergic neurotransmitter release in DSM cells [18]. During the generation of action potentials and membrane depolarization, we rigorously assessed the stability, robustness, and flexibility of our mathematical model, following the methods outlined in the Methods section. Furthermore, we validated our model-generated action potentials to evaluate its accuracy against the limited available experimental data. Upon incorporating all ion channel models, we aimed to maintain the physiological resting membrane potential (RMP) value at -52 mV. Our model’s robustness was confirmed by sustaining the RMP at -52 mV for 1000 ms (see Figure 4). However, at 0 ms, the model required a few milliseconds to stabilize due to

the instability of all ion channels, resulting in some membrane potential fluctuations. As shown in Figure 4, the time scale (x-axis) starts from 500 ms to exclude these fluctuations.

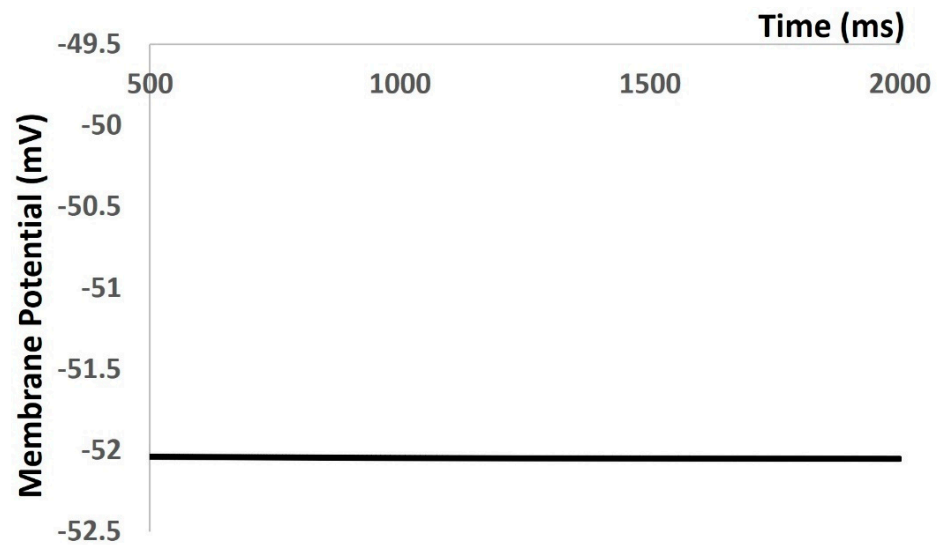


Figure 4. Model simulation shows that RMP was maintained at -52 mV.

We applied the current stimuli of various amplitudes for a duration of 10 ms to explore the evoked depolarization, action potential (AP), and threshold prediction. No spikes occurred until the stimulus reached 0.55 mA, at which point the AP was generated. Analyzing the AP (depicted by the red solid line in Figure 5) and depolarization (represented by the black solid line in Figure 5) enabled the prediction of the threshold required to trigger the AP, estimated at -38.36 mV.

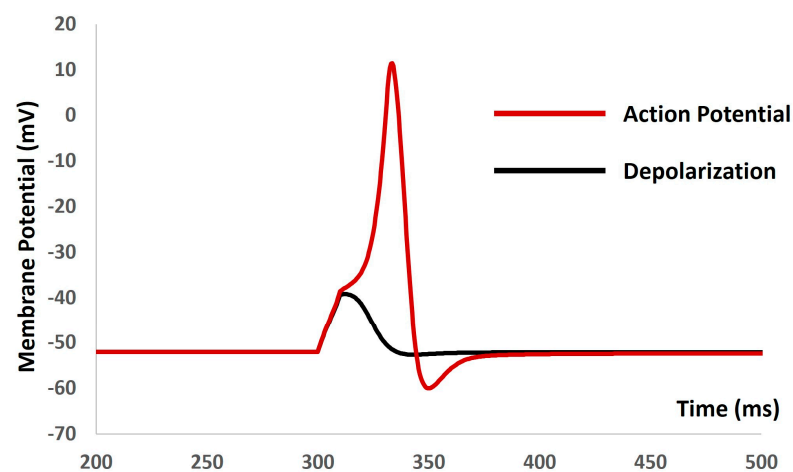


Figure 5. The model shows the AP (red line) and depolarization (black line) with the current stimulus.

We then introduced the synaptic input of various amplitudes to investigate evoked depolarization, action potentials (APs), and threshold prediction. No spikes occurred with a stimulus of $0.0076 \mu\text{S}$, whereas an AP was generated with a stimulus of $0.0077 \mu\text{S}$. Analyzing the simulated AP (depicted by the red solid line in Figure 6) and simulated depolarization (shown as the black solid line in Figure 6) predicted the threshold that needed to be met to trigger the AP at -38.42 mV. Mahapatra et al. (2018) [35] published an experimental AP in mouse DSM cells for identifying the synaptic stimulus. By comparing the extracted data from this experimental AP (illustrated by the blue dashed line in Figure 6) with our model-simulated AP, we found a good match, supporting the accuracy of our model.

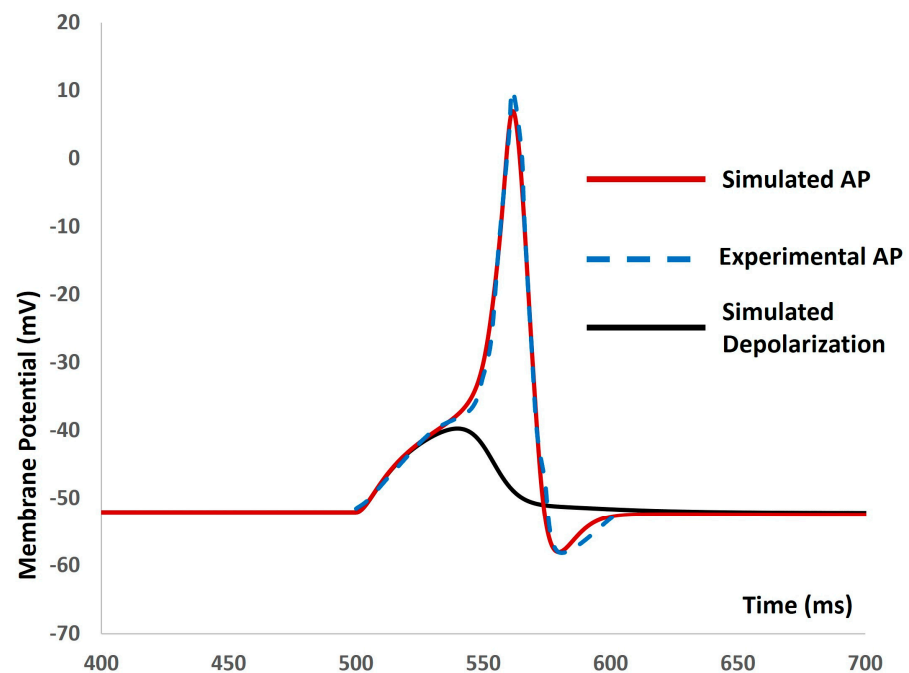


Figure 6. The model shows the simulated AP (red line), experimental AP (blue line), and simulated depolarization (black line) with synaptic input stimulus.

We then repeated our model to generate Figures 4–6 with the addition of stochastic synaptic background conductance noise. The value of $g_{ex}(t)$ in Equation (1) was varied to investigate fluctuations in the RMP with synaptic background conductance noise. Figure 7 shows the membrane potential with a value of 0.012 mho. The RMP fluctuated between -51.43 mV and -60.26 mV.

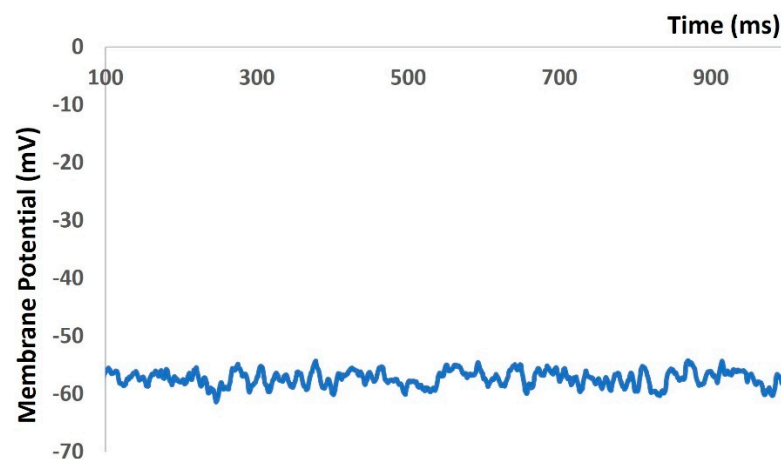


Figure 7. Model-generated RMP fluctuated with synaptic background conductance noise.

We applied the current stimulus of various amplitudes for a 10 ms duration to investigate the current evoked depolarization, AP, and threshold prediction with stochastic synaptic background conductance noise. When a stimulus of 1.9 mA was reached, there were no spikes, and, with 2 mA, the AP was generated. Based on the AP (red solid line in Figure 8) and depolarization (black solid line in Figure 8), the threshold to trigger the AP was predicted at -34.68 mV.

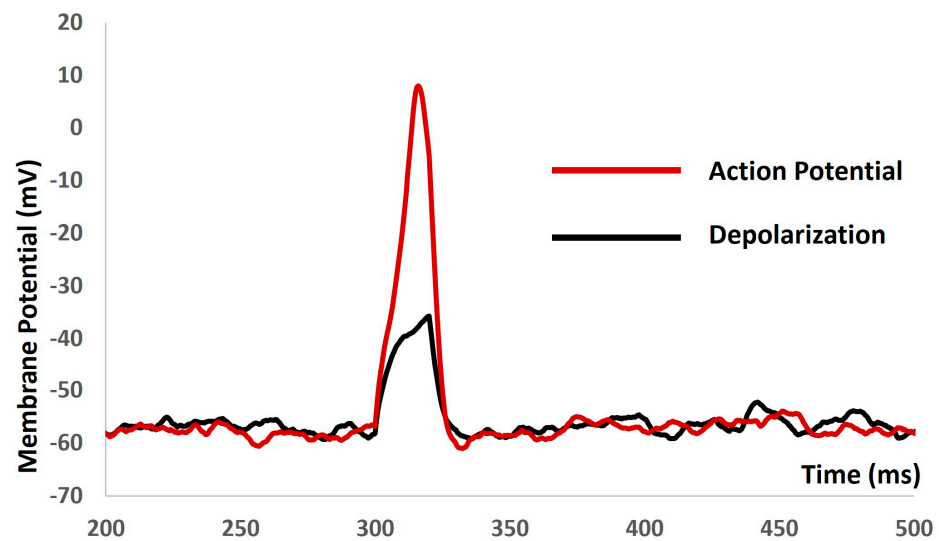


Figure 8. The model shows the AP (red line) and depolarization (black line) with current stimulus and synaptic background conductance noise.

We then introduced the synaptic input of various amplitudes to investigate the evoked depolarization, AP, and threshold prediction with stochastic synaptic background conductance noise. Figure 9 shows that with the stimuli of $0.05 \mu\text{S}$ (black solid line), $0.09 \mu\text{S}$ (blue solid line), and $0.5 \mu\text{S}$ (red solid line), there were no spikes. There were no methods to predict the threshold potential due to the absence of action potentials. The input resistance was altered significantly, and the model failed to generate any APs. The active components of the biophysical system were disabled, resulting in the system only exhibiting passive properties.

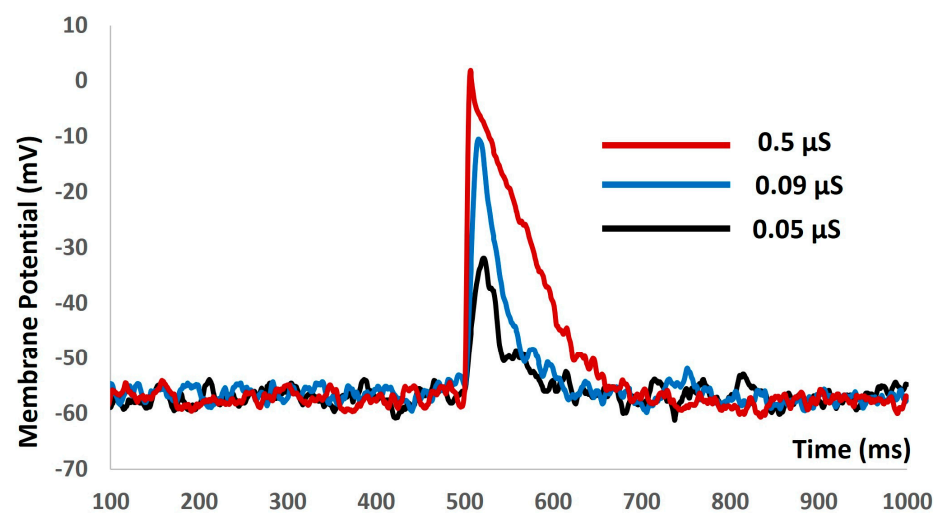


Figure 9. The model shows the evoked response for synaptic inputs with synaptic background conductance noise.

When we increased the value of $g_{\text{ex}}(t)$ in Equation (1) to more positive values, the model started to generate spontaneous depolarizations and spontaneous APs (red solid lines in Figure 10) without any current or synaptic stimulus. To explore the active properties of all ion channels, we set the conductances of both L-type and T-type calcium channels to zero. As anticipated, this manipulation resulted in a reduction in the active component of the membrane potential, as depicted by the black solid lines in Figure 10.

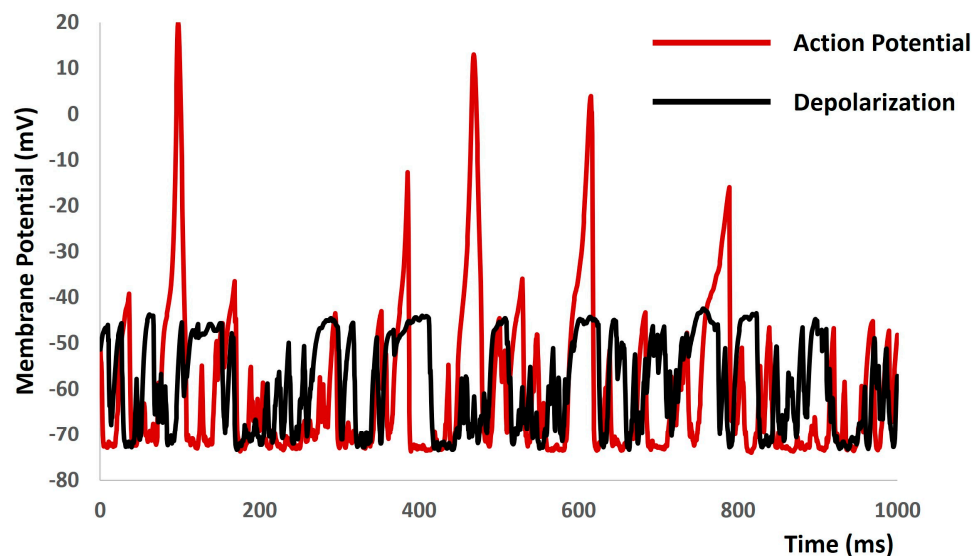


Figure 10. The model demonstrates spontaneous action potential generation under conditions of increased noise, along with the application of blockers for L-type and T-type calcium channels.

4. Discussion

Electrically excitable cells trigger membrane depolarization, initiating the generation of action potentials that initiate numerous physiological processes and facilitate intercellular communication. Neurotransmitters are released in response to stimuli or spontaneously, increasing excitatory synaptic conductance and leading to membrane depolarization. The nervous system extensively innervates excitable cells, and these mechanisms play critical roles in various pathological conditions. Neurotransmitters are released sporadically, generating electrical activity observed as background events in excitable cell recordings. Studies have investigated synaptic background activity using *in vivo*, *in vitro*, and *in silico* approaches. However, non-neuronal excitatory cells, such as smooth muscle cells, which also receive neurotransmitter-based innervation, have not been thoroughly investigated. To address this gap, we developed the first mathematical model of detrusor smooth muscle cells to examine noise in the membrane potential associated with excitatory synaptic conductance in the context of urinary incontinence. Mathematical modeling approaches are crucial for quantitatively assessing intricate biological systems, allowing for the simulation of intracellular electrophysiological activity. Our model reproduces spontaneous depolarization and action potential generation observed in experimental recordings by emphasizing the electrophysiological characteristics of detrusor smooth muscle cells.

The validation of a biophysically detailed computational model against experimental data is crucial for several reasons. Firstly, it ensures that the model accurately represents the underlying biological processes and mechanisms. Secondly, validation provides confidence in the predictive capability of the model, indicating its reliability for making predictions in real-world scenarios. This iterative process of validation and refinement enhances the model's accuracy and relevance, making it a valuable tool for understanding complex biological systems and informing experimental design and interpretation. However, validating all outputs from a computational model can be challenging due to a lack of sufficient experimental data. Without comprehensive experimental datasets for comparison, it is difficult to assess the accuracy of every aspect of the model's outputs. This limitation may lead to uncertainties in certain predictions or outputs, particularly in areas where experimental validation is lacking or impractical. In our model, we aimed to validate its numerical stability, robustness, reproducibility, and accuracy predictions by comparing them with the limited available experimental data. Although the simulated action potential and depolarization characteristics responded predictably to alterations in ion channel conductances in the physiological ranges, the action potential maintained its integrity without

experiencing any pathological deviations in amplitude or waveform parameters, thereby avoiding model breakdown. This supports the notion that our model is robust and suitable for future enhancements, including the incorporation of additional cellular and subcellular mechanisms. Figure 4 supports the claim that our model can indefinitely maintain the resting membrane potential within the physiological range observed in experiments, provided that the cell is not stimulated by any external stimulus. Figures 5 and 6 illustrate that our model can trigger an action potential when stimulated by either a strong current or synaptic input, raising the membrane potential above the threshold value. This indicates that our model has the potential to be utilized as an *in silico* experimental platform for further biophysical inquiries. In addition, Figure 6 provides further confirmation of the accuracy of our model, as it generates an action potential that closely aligns with the experimental data.

The central aim of computational modeling is also to forecast new biological and pharmacological insights inaccessible through experiments due to their intricate nature. Figures 7–10 derived from our model simulation depict new biological insights regarding the electrical excitability of smooth muscle cells. This finding further reinforces the idea that inhibitors of synaptic inputs, including ATP and acetylcholine, could act as new pharmacological targets for preventing urinary incontinence. The simulation presented in Figure 10 illustrates that random depolarization initiates the activation sequence of T-type Ca^{2+} channels, succeeded by L-type Ca^{2+} channels, ultimately leading to action potential generation. Afterward, various potassium channels activate to repolarize the membrane potential to its resting-state post-action potential. Consequently, the model accurately reproduces the impacts of T-type and L-type Ca^{2+} channel blockers, resulting in membrane voltage fluctuations of roughly a few millivolts. The evidence suggests that T-type and L-type Ca^{2+} channel blockers may serve as innovative pharmacological targets for mitigating urinary incontinence.

The inhibitory spontaneous synaptic background noise affects cellular excitability in neuronal cells. Spontaneous hyperpolarizations are observed in detrusor smooth muscle cells, likely due to this synaptic noise [43]. However, our current model cannot explore these phenomena. Stochastic ion channel activations contribute to membrane potential fluctuations and cellular excitability modulation, but our model cannot elucidate their mechanisms. Nonetheless, upgrading the model with additional mechanisms could facilitate such investigations.

In conclusion, we successfully established a computational model to analyze the dynamics of stochastic synaptic background noise in non-neuronal cells (like detrusor smooth muscle cells). This initial model will aid in comprehending additional electrophysiological traits through future enhancements. Furthermore, it will pave the way for exploring novel pharmacological interventions for urinary incontinence.

Author Contributions: Conceptualization, C.M. and I.S.; methodology, C.M. and I.S.; software, C.M. and I.S.; validation, C.M. and I.S.; formal analysis, C.M. and I.S.; investigation, C.M. and I.S.; resources, C.M. and I.S.; data curation, C.M. and I.S.; writing—original draft preparation, C.M.; writing—review and editing, C.M. and I.S.; visualization, C.M. and I.S.; supervision, I.S.; project administration, C.M. and I.S.; funding acquisition, I.S. All authors have read and agreed to the published version of the manuscript.

Funding: This research received no external funding.

Data Availability Statement: Data available within the manuscript.

Acknowledgments: The authors would like to thank the reviewers for their fruitful comments and suggestions for improving the manuscript.

Conflicts of Interest: The authors declare no conflicts of interests.

References

1. Kadir, L.A.; Stacey, M.; Barrett-Jolley, R. Emerging Roles of the Membrane Potential: Action Beyond the Action Potential. *Front. Physiol.* **2018**, *9*, 1661. [[CrossRef](#)] [[PubMed](#)]
2. Platkiewicz, J.; Brette, R. A threshold equation for action potential initiation. *PLoS Comput. Biol.* **2010**, *6*, e1000850. [[CrossRef](#)] [[PubMed](#)]
3. Schneidman, E.; Freedman, B.; Segev, I. Ion channel stochasticity may be critical in determining the reliability and precision of spike timing. *Neural Comput.* **1998**, *10*, 1679–1703. [[CrossRef](#)] [[PubMed](#)]
4. Petkov, G.V. Ion channels. In *Pharmacology*; Academic Press: Cambridge, MA, USA, 2009; pp. 387–427.
5. Kim, D.M.; Nimigean, C.M. Voltage-gated potassium channels: A structural examination of selectivity and gating. *Cold Spring Harb. Perspect. Biol.* **2016**, *8*, a029231. [[CrossRef](#)]
6. Thorneloe, K.S.; Nelson, M.T. KST Ion channels in smooth muscle: Regulators of intracellular calcium and contractility. *Can. J. Physiol. Pharmacol.* **2005**, *83*, 215–242. [[CrossRef](#)] [[PubMed](#)]
7. Amberg, G.C.; Koh, S.D.; Imaizumi, Y.; Ohya, S.; Sanders, K.M. A-type potassium currents in smooth muscle. *Am. J. Physiol. -Cell Physiol.* **2003**, *284*, C583–C595. [[CrossRef](#)] [[PubMed](#)]
8. Nielsen, M.S.; Axelsen, L.N.; Sorgen, P.L.; Verma, V.; Delmar, M.; Holstein-Rathlou, N.H. Gap junctions. *Compr. Physiol.* **2012**, *2*, 1981–2035. [[CrossRef](#)] [[PubMed](#)]
9. He, P.; Deng, J.; Zhong, X.; Zhou, Z.; Song, B.; Li, L. Identification of a hyperpolarization-activated cyclic nucleotide-gated channel and its subtypes in the urinary bladder of the rat. *Urology* **2012**, *79*, 1411.e7–1411.e13. [[CrossRef](#)]
10. Kavalali, E.T. The mechanisms and functions of spontaneous neurotransmitter release. *Nat. Rev. Neurosci.* **2015**, *16*, 5–16. [[CrossRef](#)]
11. Faisal, A.A. Stochastic simulation of neurons, axons, and action potentials. In *Stochastic Methods in Neuroscience*; Oxford University Press: Oxford, UK, 2010; pp. 297–343.
12. Yarom, Y.; Hounsgaard, J. Voltage fluctuations in neurons: Signal or noise? *Physiol. Rev.* **2011**, *91*, 917–929. [[CrossRef](#)]
13. Rusakov, D.A.; Savtchenko, L.P.; Latham, P.E. Noisy synaptic conductance: Bug or a feature? *Trends Neurosci.* **2020**, *43*, 363–372. [[CrossRef](#)]
14. Yu, H.; Dhingra, R.R.; Dick, T.E.; Galán, R.F. Effects of ion channel noise on neural circuits: An application to the respiratory pattern generator to investigate breathing variability. *J. Neurophysiol.* **2017**, *117*, 230–242. [[CrossRef](#)] [[PubMed](#)]
15. Linaro, D.; Storace, M.; Giugliano, M. Accurate and fast simulation of channel noise in conductance-based model neurons by diffusion approximation. *PLoS Comput. Biol.* **2011**, *7*, e1001102. [[CrossRef](#)]
16. Brading, A.F. Spontaneous activity of lower Urinary tract smooth muscles: Correlation between ion channels and tissue function. *J. Physiol.* **2006**, *570*, 13–22. [[CrossRef](#)] [[PubMed](#)]
17. Gabella, G. Structure of the intramural nerves of the rat bladder. *J. Neurocytol.* **1999**, *28*, 615–637. [[CrossRef](#)]
18. Young, J.S.; Meng, E.; Cunnane, T.C.; Brain, K.L. Spontaneous purinergic neurotransmission in the mouse urinary bladder. *J. Physiol.* **2008**, *586*, 5743–5755. [[CrossRef](#)]
19. Smith, A.C.; Hristov, K.L.; Cheng, Q.; Xin, W.; Parajuli, S.P.; Earley, S.; Malysz, J.; Petkov, G.V.; Hamilton, K.L.; Rovner, E.S.; et al. Novel role for the transient potential receptor melastatin 4 channel in guinea pig detrusor smooth muscle physiology. *Am. J. Physiol.-Cell Physiol.* **2013**, *304*, C467–C477. [[CrossRef](#)]
20. Parajuli, S.P.; Soder, R.P.; Hristov, K.L.; Petkov, G.V. Pharmacological activation of small conductance calcium-activated potassium channels with naphtho [1, 2-d] thiazol-2-ylamine decreases guinea pig detrusor smooth muscle excitability and contractility. *J. Pharmacol. Exp. Ther.* **2012**, *340*, 114–123. [[CrossRef](#)]
21. Heppner, T.J.; Bonev, A.D.; Nelson, M.T. Elementary purinergic Ca²⁺ transients evoked by nerve stimulation in rat urinary bladder smooth muscle. *J. Physiol.* **2005**, *564*, 201–212. [[CrossRef](#)] [[PubMed](#)]
22. Brading, A.F.; Brain, K.L. Ion channel modulators and urinary tract function. In *Handbook of Experimental Pharmacology*; Springer: Berlin/Heidelberg, Germany, 2011; pp. 375–393.
23. Meng, E.; Young, J.S.; Brading, A.F. Spontaneous activity of mouse detrusor smooth muscle and the effects of the urothelium. *Neurourol. Urodyn.* **2008**, *27*, 79–87. [[CrossRef](#)] [[PubMed](#)]
24. Mahapatra, C.; Brain, K.; Manchanda, R. Biophysically Realistic Models of Detrusor Ion Channels: Role in shaping spike and excitability. In *Urinary Bladder Physiology: Computational Insights*; Publ Narosa Publishing House: New Delhi, India, 2024.
25. Sui, G.; Wu, C.; Severs, N.; Newgreen, D.; Fry, C.H. The association between T-type Ca²⁺ current and outward current in isolated human detrusor cells from stable and overactive bladders. *BJU Int.* **2007**, *99*, 436–441. [[CrossRef](#)] [[PubMed](#)]
26. Hikaru, H.; Brading, A.F. Ionic basis for the regulation of spontaneous excitation in detrusor smooth muscle cells of the guinea-pig urinary bladder. *Br. J. Pharmacol.* **2003**, *140*, 159–169. [[CrossRef](#)]
27. Fry, C.H.; Sui, G.-P.; Severs, N.J.; Wu, C. Spontaneous activity and electrical coupling in human detrusor smooth muscle: Implications for detrusor overactivity? *Urology* **2004**, *63*, 3–10. [[CrossRef](#)] [[PubMed](#)]
28. Mogilner, A.; Wollman, R.; Marshall, W.F. Quantitative modeling in cell biology: What is it good for? *Dev. Cell* **2006**, *11*, 279–287. [[CrossRef](#)]
29. Vagos, M.; van Herck, I.G.; Sundnes, J.; Arevalo, H.J.; Edwards, A.G.; Koivumäki, J.T. Computational modeling of electrophysiology and pharmacotherapy of atrial fibrillation: Recent advances and future challenges. *Front. Physiol.* **2018**, *9*, 1221. [[CrossRef](#)] [[PubMed](#)]

30. Rinzel, J.; Huguet, G. Nonlinear dynamics of neuronal excitability, oscillations, and coincidence detection. *Commun. Pure Appl. Math.* **2013**, *66*, 1464–1494. [[CrossRef](#)] [[PubMed](#)]
31. Rekling, J.C.; Funk, G.D.; Bayliss, D.A.; Dong, X.-W.; Feldman, J.L.; Ansdell, P.; Brownstein, C.G.; Škarabot, J.; Hicks, K.M.; Simoes, D.C.M.; et al. Synaptic control of motoneuronal excitability. *Physiol. Rev.* **2000**, *80*, 767–852. [[CrossRef](#)]
32. Zhu, R.J.; Wei, X.X. Unsupervised approach to decomposing neural tuning variability. *Nat. Commun.* **2023**, *14*, 2298. [[CrossRef](#)] [[PubMed](#)]
33. Pirozzi, E. Colored noise and a stochastic fractional model for correlated inputs and adaptation in neuronal firing. *Biol. Cybern.* **2018**, *112*, 25–39. [[CrossRef](#)] [[PubMed](#)]
34. Fellous, J.M.; Rudolph, M.; Destexhe, A.; Sejnowski, T.J. Synaptic background noise controls the input/output characteristics of single cells in an in vitro model of in vivo activity. *Neuroscience* **2003**, *122*, 811–829. [[CrossRef](#)]
35. Mahapatra, C.; Brain, K.L.; Manchanda, R. A biophysically constrained computational model of the action potential of mouse urinary bladder smooth muscle. *PLoS ONE* **2018**, *13*, e0200712. [[CrossRef](#)]
36. Mahapatra, C.; Brain, K.L.; Manchanda, R. Computational studies on urinary bladder smooth muscle: Modeling ion channels and their role in generating electrical activity. In Proceedings of the 2015 7th International IEEE/EMBS Conference on Neural Engineering (NER), Montpellier, France, 22–24 April 2015; pp. 832–835.
37. Dave, V.; Mahapatra, C.; Manchanda, R. A mathematical model of the calcium transient in urinary bladder smooth muscle cells. In Proceedings of the 2015 37th Annual International Conference of the IEEE Engineering in Medicine and Biology Society (EMBC), Milan, Italy, 25–29 August 2015; pp. 5359–5362.
38. Mahapatra, C.; Brain, K.L.; Manchanda, R. Computational study of ATP gated Potassium ion channel in the urinary bladder over activity. In Proceedings of the 2016 International Conference on Inventive Computation Technologies (ICICT), Coimbatore, India, 26–27 August 2016; Volume 2, pp. 1–4.
39. Mahapatra, C.; Dave, V.; Manchanda, R. A Mathematical Modeling of Voltage-gated Calcium ion channel based Calcium Transient Response in UrinaryBladder Smooth Muscle Cell. *Int. J. Pure Appl. Math.* **2017**, *117*, 71–75.
40. Hodgkin, A.L.; Huxley, A.F. A quantitative description of membrane current and its application to conduction and excitation in nerve. *J. Physiol.* **1952**, *117*, 500. [[CrossRef](#)]
41. Fry, C.H.; Cooklin, M.; Birns, J.; Mundy, A.R. Measurement of intercellular electrical coupling in guinea-pig detrusor smooth muscle. *J. Urol.* **1999**, *161*, 660–664. [[CrossRef](#)] [[PubMed](#)]
42. Hines, M.L.; Carnevale, N.T. The NEURON simulation environment. *Neural Comput.* **1997**, *9*, 1179–1209. [[CrossRef](#)]
43. Mahapatra, C.; Kumar, R. Biophysical Mechanisms of Vaginal Smooth Muscle Contraction: Role of the Membrane Potential and Ion Channels. *Preprints* **2024**, *2024*, 2024031690. [[CrossRef](#)]

Disclaimer/Publisher’s Note: The statements, opinions and data contained in all publications are solely those of the individual author(s) and contributor(s) and not of MDPI and/or the editor(s). MDPI and/or the editor(s) disclaim responsibility for any injury to people or property resulting from any ideas, methods, instructions or products referred to in the content.